Coster-Kronig decay of 3p core-excited states of atomic zinc

M. Y. Adam, S. Stranges,* M. de Simone,* S. Svensson,† and F. Combet Farnoux‡
Laboratoire pour l'utilisation du Rayonnement Electromagnétique, Bâtiment 209 D, Université Paris-Sud, 91405 Orsay Cedex, France

(Received 12 February 1993; revised manuscript received 7 September 1993)

By exciting the *M* shell of atomic zinc in the 80–110-eV photon energy range with synchrotron radiation, and by using photoelectron and photoion detection, we have located the $3p^5 3d^{10} 4s^2 ns$ (and *nd*) excited states in the 91–99-eV region. Resonant satellites are observed, allowing us to demonstrate the dominant role played by the $3p^{-1} ns^1 \rightarrow 3d^{-2} n'l\varepsilon f$ interaction upon the decay of the $3p \rightarrow ns$ excited states. The $3p^{-1} ns^1 \rightarrow 3d^{-2} n'l\varepsilon f$ super-Coster-Kronig processes produce a large broadening of the 3*p* excited states which form series of overlapping states. The resonant satellites lying in the high-energy region are singly ionized states of $3p^6 3d^8 4s^2 n'l$ configurations, which autoionize into the various $3p^6 3d^9 4p$ or $3p^6 3d^9 4s$ states of Zn^{2+}. *Ab initio* calculations using intermediate coupling have been performed and display good quantitative agreement with the experimental results.

PACS number(s): 32.80.Hd, 32.80.Fb, 32.80.Dz, 31.50.+w

INTRODUCTION

Sonntag and Zimmermann [1] have reviewed the extreme-ultraviolet spectroscopy of metal atoms. This review shows that for the 3*d* transition metals, as long as the 3*d* shell is unfilled, the lowest members of the Rydberg series of 3*p* core-excited states are followed by an autoionization in the $4s^{-1}$ or $3d^{-1}$ valence channels, resulting in a strong enhancement of the singly-charged-ion signal. Super-Coster-Kronig decay processes are also involved, following a $3p \rightarrow ns$ or $3p \rightarrow nd$ transition in a 3*d* transition metal, but they are not the dominant deexcitation process. By contrast, such super-Coster-Kronig processes control the deexcitation of the 3*p* excited states when the 3*d* shell is full. This is known [1] to be the case for the decay of the core-excited "valence" state $3p \rightarrow 4s$ (transition to the 4*s* unfilled valence shell) in atomic Cu ($3p^6 3d^{10} 4s\ ^2S$). Upon such a decay, the interpretations [2,3] of the prominent resonant satellite channels that can be observed in the electron spectra [4,5] below the first double-ionization thresholds assume that the excited 4*s* electron is a spectator of the $3p^{-1} 4s \rightarrow 3d^{-2} 4s\varepsilon f$ interaction. An enhancement of the singly-charged-ion signal results.

For atomic zinc ($3p^6 3d^{10} 4s^2\ ^1S$), the 4*s* shell is full, and as a consequence the three following spectroscopic features may be emphasized: (i) a large difference (15 eV) between the $3p^{-1}$ (^2P) thresholds, lying at approximately 81.5 and 83.1 eV in Cu [6] and 96.1 and 98.7 eV in zinc [7]; (ii) almost identical values for the double-ionization onset lying at 28 eV in copper and 27.35 eV in zinc; and (iii) a large shift between the $3d^{-2} 4s$ at 35 eV and $3d^{-2} 4s^2$ at 51 eV double-ionization thresholds in copper and zinc, respectively. These statements should be in favor of a similarity of Zn with Cu [6] in the behavior of the 3*p* core-excited-states decay (via a two-step process producing doubly charged ions), despite their large energy shifted positions for Zn comparatively to Cu. This is why one of the major aims of the present work lies in showing that for Zn where both 3*d* and 4*s* shells are full, the 3*p* core-excited-states deexcitation is controlled by the super-Coster-Kronig processes $3p^{-1} ns^1 \rightarrow 3d^{-2} n'l\varepsilon f$ ($n' \geq n$), which preferentially produce doubly charged ions.

By contrast, the preferential production of multiply charged ions ($n = 3$ or 4) has been observed already [8] by ion spectroscopy in the cases of 3*p* and 4*p* core-excited-states decay in Kr and Xe, respectively. This different behavior could be due to the existence of Coster-Kronig processes within the p^6 valence shell of the rare gases.

Because of its full-shell structure and its high vapor pressure, zinc has been the subject of numerous theoretical and experimental investigations. Ohno and Wendin [7] were the first to propose a many-body treatment of the 3*p* x-ray photoelectron spectrum (XPS) and super-Coster-Kronig (SCK) electron spectrum [9] of atomic Zn. Other calculations [10] have been achieved within an independent particle model. Fliflet and Kelly [11] predicted intense autoionizing resonances in the $3d \rightarrow \varepsilon f$ cross section due to the $3p^5 3d^{10} s^2 ns$ ($n \geq 5$) configurations. According to these calculations, we would expect a large increase of the Zn^+ yield when a 3*p* core electron is excited. Photoabsorption [12] and total photoionization studies [13] of zinc are numerous up to 36-eV photoexcitation energy and the single- and double-ionization yield measurements [14,15] were known up to 65 eV. A recent ex-

*Permanent address: Dipartimento di Chimica, Università degli Studi di Roma "La Sapienza", P. le A. Moro 5, 00185 Rome, Italy.
†Permanent address: Institute of Physics, Box 530 Uppsala University, S-751 21 Uppsala, Sweden.
‡Permanent address: Laboratoire de Photophysique Moléculaire du CNRS, Bât. 213, Université Paris-Sud, 91405 Orsay, France.

perimental reinvestigation of the 4s, 3d, and 3p partial-photoionization cross sections [16,17] has confirmed the predictions [11,18] that the 3d cross section is largely dominant (more than 80% of the total photoionization cross section) for photoexcitation energy ranging from 25 up to 110 eV.

The present paper also reports *ab initio* calculations relative to the position of both various excited states of $3p^5 3d^{10} 4s^2 ns$ ($n \geq 5$) and $n'd$ ($n' \geq 4$) configurations and 3p thresholds. The oscillator strengths of the corresponding transitions have been determined within the same approximations.

EXPERIMENT

The photoelectron emission measurements as well as the single- and double-photoionization yield measurements were performed at the SUPERACO positron storage ring at Orsay with the setups already described [19,20]. A grazing-incidence toroidal monochromator equipped with a 450- and 1200-grooves/mm grating disperses the synchrotron radiation in the 80–115-eV range with a negligible contribution of the second order. A gold-mesh photodiode monitored the photon-beam intensity and its value was automatically stored.

The photoelectron spectrometer and the furnace were similar to previous versions described in details in Refs. [17,19]. Photoelectron spectra (PES) were recorded using a 127° cylindrical analyzer operated in a constant-pass-energy mode. Its resolution was set at 0.3 eV or ≈ 0.7 eV. The detection angle was set to the magic angle that eliminates angular distribution effects. Using the constant-pass-energy mode we have the ability to record either a constant-ionic-state spectrum (CISS), which provides the partial-photoionization cross section versus photon energy for a final ionic state with a well-known binding energy E_b, or a constant-kinetic-energy spectrum (CKES). In both cases, CISS and CKES, the photon energy is continuously scanned. In recording CISS, one varies simultaneously $h\nu$ and the retardation voltage applied on the electron spectrometer (i.e., the electron energy E_k) thereby satisfying the equation $E_b = h\nu - E_k$. In recording CKES, one sets the electron energy constant.

For the single- and double-photoionization yield measurements the dispersed synchrotron beam (bandwidth ≈ 0.1–0.3 eV) was focused onto the interaction zone set ≈ 10 mm from the exit of a graphite cell resistively heated to produce a beam of atomic Zn. Ions were detected with a time-of-flight (TOF) mass spectrometer. We had the ability either to record total ion yield versus photon energy or, at a fixed photon energy, to record a time-of-flight spectrum. Time-of-flight spectra are displayed in Fig. 1. TOF provide for the Zn^{2+}-to-Zn^+ and Zn^{3+}-to-Zn^+ ratios and the Zn^+ yield curve relative to the fairly well-known He^+ 1s photoionization cross section. For that purpose, a constant pressure of He is added in the ionization region in order to check at a fixed 100-eV excitation energy the stability of the zinc vapor pressure. Finally, our measurements are displayed in Fig. 2 as Zn^+, Zn^{2+}, and total ion-yield curves. The relative Zn^{2+} cross section is the product of the relative Zn^+ cross section and the Zn^{2+}-to-Zn^+ ratio.

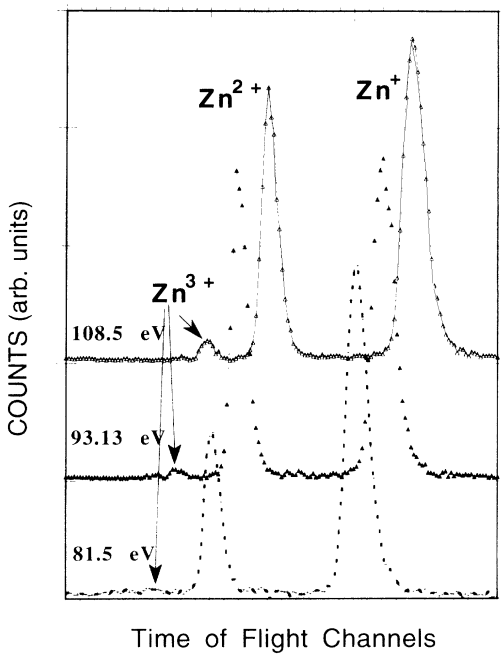

FIG. 1. Typical time-of-flight (TOF) spectra recorded at several photon energies. For clarity of the lecture the spectra at 93.13 and 108.5 eV have been shifted in both scales. The spectra are normalized to the total number of ions. Peak areas give the contributions of the singly and multiply charged ions.

AB INITIO CALCULATIONS

We have supposed that the $3p^6 3d^{10} 4s^2 ({}^1S)$ configuration describes correctly the ground state ($J=0$). In order to determine both the position of the excited states $3p^5 3d^{10} 4s^2 ns$, $n'd$, and the oscillator strengths of the corresponding transitions, we have used the intermediate-coupling approximation to diagonalize the $J=1$ energy matrix. This energy matrix is built from a basis including both $3p^5 3d^{10} 4s^2 ns$ and $3p^5 3d^{10} 4s^2 n'd$ states (n and n' represent both discrete and continuum excitations covering up to about 2 Rydbergs above the 3p thresholds). The radial basis wave functions are obtained within the averaged Hartree-Fock approximation. One major advantage of this method lies in a consistent location of both the 3p thresholds and the various terms of the series converging on them. This theoretical study is, as far as we know, the only one to take into account the mixing of both triplets and singlets which describes each term of a series. Using the intermediate-coupling approximation leads to diagonalizing a matrix including the electrostatic interaction and the spin-orbit splitting for the transition $J=0$ to $J=1$. Because of the very small value of the exchange integral $G^1(3p \rightarrow 5s)$ our intermediate-coupling results are very close to what a j-j coupling calculation would give, i.e., 66% ${}^1P_1$ and 34% ${}^3P_1$ for the series converging to the ${}^2P_{3/2}$, and the reverse for the second series, converging to the ${}^2P_{1/2}$ threshold.

RESULTS AND DISCUSSION

Some photoemission results are shown in Fig. 2. Curves *b* and *c* display the constant-ionic-state spectrum

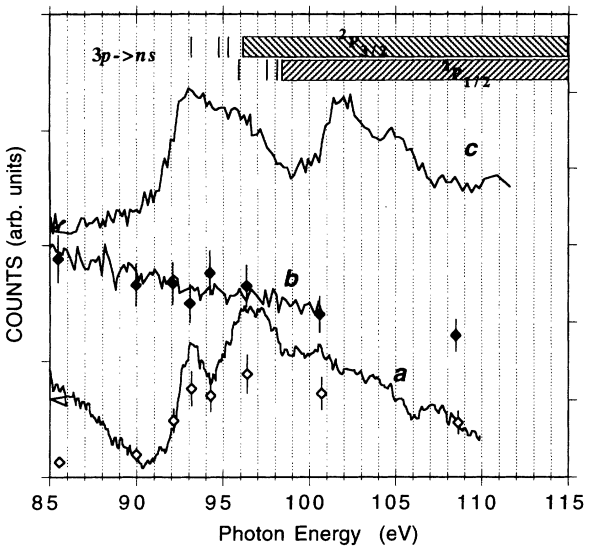

FIG. 2. Solid diamond: relative variation of the Zn^+ ion yield; open diamond: relative Zn^{2+} ion yield; curve *a*: total ion yield; curve *b*: constant-ionic- (final-) state spectrum (CIS) of the $3d^{-1}$ photo line; curve *c*: constant-kinetic-energy spectrum (CKES) recorded at a 5.60±0.35-eV electron energy, with a 0.3–0.5-eV photon bandwidth in the 82–112-eV range. The tick marks indicate the $(Z+1)$ resonance energies of $3p \rightarrow ns$ ($n=5$–7): see Table I, columns 3 and 4. The hatched horizontal bars locate the continua with $3p^{-1}(^2P_{3/2,1/2})\varepsilon l$ configurations and threshold values at 96.1 and 98.9 eV determined in the present work by analyzing curve *c* (see Results and Discussion).

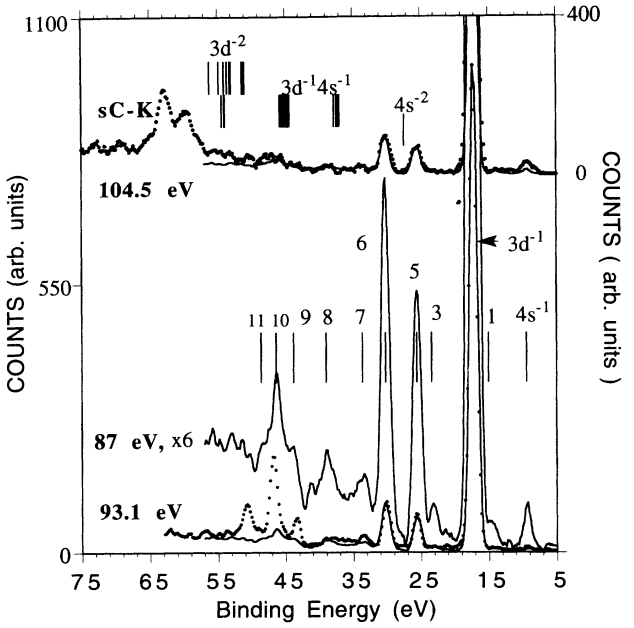

FIG. 3. Atomic zinc photoelectron spectra. The upper part refers to the ordinate on the right. Solid line: PES recorded at 87 eV; dotted line: PES at 104.5 eV; the tick marks locate the position of the Zn^{2+} levels obtained from Moore [21] or Crooker and Dick [23]. The bottom part refers to the ordinate on the left. Solid lines: PES at 87 eV with magnification 1 and 6; dotted line: PES at 93.1 eV. All the spectra are normalized to the $3d^{-1}$ mainline both in position and intensity.

of the $3d^{-1}$ main line, and the constant-kinetic-energy spectrum for 5.6-eV electron energy. Curve *c* shows two large structures in the 91–97-eV and 100–107-eV energy region that are easily explained. The second structure is due to the $3p^{-1}{}^2(P_{3/2,1/2})$ photolines which appear at 5.6-eV kinetic energy when the photon energy is scanned in the corresponding range. In fact, by an appropriate deconvolution of this structure observed in the 100–107-eV region, we have obtained the 3*p* binding energies at 96.1 and 98.9 eV, in very good agreement with the experimental values, 96.1 and 98.7 eV, respectively, found in the literature [9]. This deconvolution is obtained with a 2.3-eV and 2.2-eV linewidth, respectively, for the two components. This 2.2-eV linewidth of the 3*p* levels is in agreement with the values reported by Melhorn, Breuckmann, and Hausamann [9]. Our *ab initio* calculations locate these 3*p* threshold values at 95.74 and 98.47 eV, respectively.

In the following paragraphs we will show that the photoion and photoemission data reported in Fig. 2 allow us to (a) locate the positions of the 3*p* excited states, (b) prove that they form series of overlapping states, and (c) show that the final products of the 3*p* excited states decay are exclusively doubly charged ions.

In Fig. 3 are plotted together photoelectron spectra of atomic Zn recorded at different photon energies, namely, 87.00±0.35, 93.10±0.35, and 104.5±0.5 eV. The energy resolution of the electron spectrometer was set at roughly 0.7 eV, providing an overall electron energy resolution which is about 1 eV, except at 104.5, for which it reaches 1.5 eV. The spectrum recorded off resonance at 87.00±0.35 eV is enhanced to show the positions of the correlation satellites, 1,3,5–11, observed by us [16] in the valence spectrum of zinc. The spectra reported in Fig. 3 are normalized to the $3d^{-1}$ mainline both in position and in intensity, and the spectrum at 87.00±0.35 eV serves as a reference for the off-resonance region. The PES recorder at 104.5±0.5 eV shows the super-Coster-Kronig electron spectrum of the $3p^{-1}(^2P_{3/2,1/2})$ core holes. It is in qualitative agreement with an earlier reported spectrum [9], since it exhibits two peaks at 41.7- and 44.7-eV electron energy.

In Fig. 4 are plotted together detailed photoelectron spectra of Zn recorded at different photon energies, namely, 90.10±0.35, 92.00±0.35, 93.10±0.35, 93.90 ±0.35, and 94.20±0.35 eV. In the following paragraphs we will show that the data displayed in Fig. 4 allow us to (a) confirm the experimental findings obtained with the results displayed in Fig. 2, and (b) discuss the validity of the spectator electron model in the deexcitation of the 3*p* core-excited states.

Location of the 3p core-excited states

The total ion yield (curve *a* in Fig. 2) shows the experimental evidence of resonant processes for atomic Zn in the 80–115-eV photon energy range. We may notice three points.

(i) The resonant enhancement observed at roughly 93 eV in the total ion yield, curve *a*, should indicate the po-

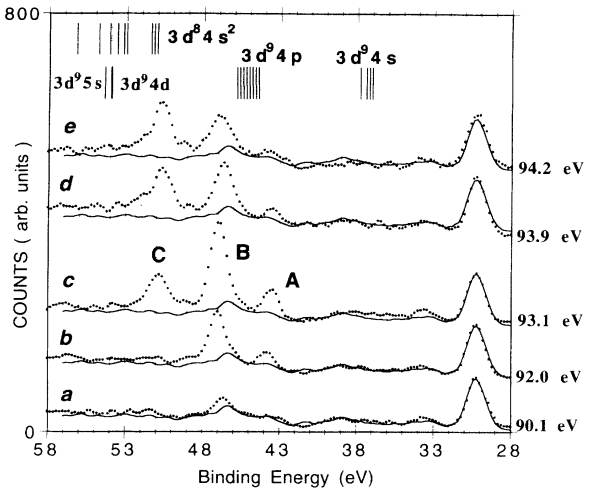

FIG. 4. Off- and on-resonance photoelectron spectra of atomic zinc (curves $a-e$). Solid line: PES at 87.00±0.35 eV, which is superimposed to the spectra displayed in curves $a-e$ by adjusting the $3d^{-1}$ mainlines, both in position and intensity. The tick marks locate the positions of the Zn^{2+} levels obtained from Moore [21] or Crooker and Dick [23].

sition of the first member $3p \rightarrow 5s$ of the series of excited states $3p \rightarrow ns$ converging to the $^2P_{3/2}$ threshold. We have several reasons to believe in this assignment. Once the calculated positions reported by Fliflet and Kelly [11] are adjusted to a more recent and realistic value of the $3p$ electron-removal energy, the position of the first $3p \rightarrow 5s$ transition is located at 93.7 eV (see Table I). Also, we found the first $3p \rightarrow 5s$ transition lying at 93.18 eV (see Table I) by using the $(Z+1)$ model. For that purpose we used the optical transitions $4p \rightarrow ns$ (^2S) and $4p \rightarrow nd$ (^1S)nd (^2D) in GaI obtained from Moore [21], and we adjust the limits of these series to the known values of the $3p$ electron binding energies in atomic zinc (see Table I). Finally, our *ab initio* calculations described above allow a more precise assignment: a first excited state is found at 92.3 eV and corresponds to the transition into $3p^5 3d^{10} 4s^2 (^2P) 5s\ ^1P_1$; this $^1P_1$ notation corresponds to the major component (66%) whereas the $^3P_1$ component is only 34% within the intermediate-coupling scheme (see Table I). These estimated values (93.7, 93.18, and 92.3 eV) for the $3p \rightarrow 5s$ transition fit well the resonant structure observed at roughly 93 eV.

(ii) The total ion yield, curve c, has been recorded with 0.1–0.15-eV, 0.15–0.3-eV, and 0.3–0.6-eV photon bandwidths, depending upon the 85–95-eV, 95–100-eV, and 100–115-eV photon energy ranges, respectively. The bandwidth in the 85–95-eV range is much smaller than the half-width of the unresolved resonant structure lying in the 90.5–94.5-eV energy range. This experimental finding may be explained if the excited-state halfwidth is larger than the spacing between the $3p \rightarrow 5s$ and $3p \rightarrow 6s$ transitions.

Evidently the $3p \rightarrow nd$ series of excited states may also contribute to the enhancement of the total ion yield around 93–94 eV. In agreement with Fliflet and Kelly [11], our calculations show that the resonances due to the transitions to the $3p^5 4s^2 nd$ configurations are negligible relative to those to the $3p^5 4s^2 ns$ configurations. Nevertheless we will discuss below a certain disagreement with these authors concerning the autoionization rates of the $3p^5 4s^2 ns$ and $3p^5 4s^2 nd$ states in the $3d \rightarrow \varepsilon f$ channel. The half-width of the excited states $^1P_1$ and $^3P_1$ with configuration $3p^5 3d^{10} 4s^2 (^2P) 5s$ is at least 1.5 eV in the total ion yield, curve c. Our calculations in Table I show that the spacing between the $3p \rightarrow 5s$ and $3p \rightarrow 6s$ transitions is roughly 1.6 eV. These conclusions imply that in zinc the $3p$ core-excited states, $3p^5 3d^{10} 4s^2 (^2P) ns$ ($n \geq 5$), form series of overlapping states. This analysis is confirmed by the resonant structures observed in the pho-

TABLE I. Calculated values for $3p \rightarrow ns$ and $3p \rightarrow nd$ resonances. Column 2: resonance energy E_n for the autoionizing $3p^5 4s^2 ns$ (and nd) configurations in the main $3d \rightarrow \varepsilon f$ and $3d \rightarrow \varepsilon p$ cross sections calculated by Fliflet and Kelly [11]. These calculations neglected the spin-orbit interaction and used a wrong experimental value for the $3p^{-1}$ threshold at 87.1 eV. Therefore we have shifted all the positions using a more realistic position at 97.13 eV obtained by taking the average of the experimental electron-removal energies $E(3p, ^2P_{3/2}) = 96.1$ eV and $E(3p, ^2P_{1/2}) = 98.8$ eV (see Results and Discussion), weighted by the $3p_{3/2}^{-1}:3p_{1/2}^{-1}$ ratio of 1.8 [7]. Columns 3 and 4: energy value in eV for the position of the $3p \rightarrow ns$ or nd transitions in atomic Zn, determined by using the $(Z+1)$ model and optical transitions in atomic Ga, obtained from Moore [21]. The series are adjusted in the energy scale to the experimental $3p^{-1}$ thresholds displayed in the same column. Columns 5 and 6: results of the present *ab initio* calculations for the position (in eV) of the excited states $3p^5 3d^{10} 4s^2 ns$ or $n'd$ ($J=1$), and the $3p$ thresholds within the intermediate-coupling scheme.

Transition	Ref. [11]	$(Z+1)$ approximation		Calculated values	
$3p \rightarrow ns$	$3p \rightarrow ns$	$3p(^2P_{3/2}) \rightarrow ns$	$3p(^2P_{1/2}) \rightarrow ns$	$3p^5 3d^{10} 4s^2 (^2P_{3/2}) ns\ ^1P_1$	$3p^5 3d^{10} 4s^2 (^2P_{1/2}) ns\ ^3P_1$
$5s$	93.7	93.18	95.98	92.3	95.01
$6s$	95.7	94.76	97.56	93.8	96.5
$7s$	96.3	95.32	98.13	94.3	97.1
$8s$				94.6	97.3
$3p \rightarrow nd$	$3p \rightarrow nd$	$3p(^2P_{3/2}) \rightarrow nd$	$3p(^2P_{1/2}) \rightarrow nd$	$3p^5 3d^{10} 4s^2 (^2P_{3/2}) nd\ ^{1,3}P_1$	$3p^5 3d^{10} 4s^2 (^2P_{1/2}) nd\ ^3D_1$
$4d$	95.5	94.41	97.21	93.5	96.20
$5d$	96.2	95.16	97.96	94.2	96.90
$6d$	96.8	95.5	98.3	94.5	97.25
$3p^{-1}$	97.13	96.1	98.9	95.74	98.47

toelectron spectra recorded on resonances and displayed in Figs. 3 and 4. This point is more extensively discussed below in the text and in the Appendix.

(iii) It is well established [1,7] that after ionization of the $3p$ shell in zinc, super-Coster-Kronig decay processes, i.e., $3p^{-1} \rightarrow 3d^{-2}\varepsilon f$, occur which lead to a large shift and broadening of a $3p$ core hole. For zinc, in spite of the large (≈ 1.5-eV) lifetime half-width of the $3p$ excited states, we may point out the difference observed between this value and the 2.2-eV lifetime half-width of the $3p$ hole [1,7,9]. Such a difference is observed in the case of copper, since Jensen *et al.* [24] measured for the $3p$ hole a 2.2 ± 0.3-eV half-width, whereas Bruhn *et al.* [25] have measured a 1.75-eV value for the half-width of the $3p$ excited "valence" state. In the case of zinc we suggest that the difference could be partly due to an observed additional decay of the $3p$ hole into the Zn^{3+} channel (see Figs. 1 and 6).

(iv) In Fig. 2, curve *a*, the large enhancement centered around 96 eV may be explained by the contributions of ^1P and ^3P excited states corresponding to a $3p \rightarrow ns$ ($n \geq 6$) electronic transition, but also by the contribution of the $3p^{-1}\,^2P_{3/2}$ partial-photoionization cross section, since the threshold of this ionic state is located at 96.1 eV.

Preferential decay of 3p core-excited states

"Zn^+" ion yield

We can notice several points by comparing the photoion and photoemission measurements reported in Figs. 2–4.

(1) It is evident from the PES displayed in Fig. 3 that the $3d^{-1}$ photoelectron line and its satellite, line 5, give the main contribution to the Zn^+ ion-yield curve in the 87–104.5-eV photon energy region.

(2) The PES displayed in Figs. 3 and 4 are normalized to the same value of the $3d^{-1}$ mainline. We find for both the off- (at 87.00 and 90.10 ± 0.35 eV) and on-resonance excitation energies (at 92.00 ± 0.35, 93.10 ± 0.35, 93.90 ± 0.35, and 94.20 ± 0.35 eV) identical values for the relative intensity of satellite 5.

(3) The $3d^{-1}$ photoionization cross section, displayed in Fig. 2, curve *b*, gradually decreases throughout the whole 82–100-eV photon energy range, quite consistently with the Zn^+ ion-yield measurements. Comparing this latter result to the experimental findings pointed out in (1) and (2), we conclude that the single photoionization cross section should decrease monotonically in the whole 91.5–94.5-eV energy range.

According to our expectations, the resonances $3p^5 4s^2 ns$ (and nd) do not decay into final singly charged states in the whole 91.5–100-eV energy range. This experimental finding is in conflict with the prediction [11] of sharp resonances in the $3d \rightarrow \varepsilon f$ partial cross section arising from autoionizing $3p^5 4s^2 ns$ and $3p^5 4s^2 nd$ configurations.

"Zn^{2+}" ion yield

The large enhancement observed in the total ion yield (Fig. 2, curve *a*) between 90 and 95 eV and centered around 93 eV, is entirely due to a corresponding enhancement shown in the Zn^{2+} ion yield reported in Fig. 2. We may point out that in our analysis we have neglected the very low contribution of the trications Zn^{3+}. This effect is shown in the time-of-flight spectra displayed in Fig. 1. This experimental finding tells us that the core-excited states $3p^5 3d^{10} 4s^2 ns$ (and nd) preferentially decay to doubly charged Zn^{2+} ions.

These states can decay via (i) autoionization of highly excited singly ionic states, (ii) resonant Auger or super-Coster-Kronig transition, and (iii) resonant shakeoff process.

(i) Autoionization of a highly excited singly ionic state as probed by satellite 6 is not observed. In all PES normalized to the $3d^{-1}$ mainline and recorded off and on resonances, we find identical values for the relative intensity of satellite 6. In Figs. 3 and 4, all the PES displayed on resonance are superimposed with a PES recorded off resonance at 87 eV. For satellites 7–11 the situation is more ambiguous since in the PES recorded at 93.1 eV we may observe a small enhancement of the signal in the 32–38-eV binding energy range. Resonant structures labelled *A*, *B*, and *C* are observed in Fig. 4, curves *b*–*e*, and they overshadow the satellites 9, 10, and 11 observed in PES recorded off resonance at 87 eV.

(ii) The large (1.5-eV) half-width of the $3p \rightarrow 5s$ resonance observed in the total ion yield, Fig. 2, curve *a*, suggests that the decay process is extremely strong, as it should be in the case of super-Coster-Kronig decay pro-

TABLE II. Binding energies and assignments for the valence photoelectron lines in the photoexcited spectra of Zn vapor. The tentative assignment of the satellites 3, 5, and 6 is based on energies from Moore's table [21] and from calculations of Cowan and Wilson [22]. According to these calculations the states corresponding to low-lying even-parity configurations should be found in the following energy ranges: $3d^9 4s 5s$ (shakeup satellites) between 29 and 30 eV, $3d^9 4s 4d$ (final-state configuration-interaction satellites) between 29.3 and 31.8 eV, and $3d^9 4p^2$ (conjugate shakeup satellites) between 29.3 and 33.3 eV. A weighted position at 17.29 eV for the $3d^{-1}\,^{3,1}D$ lines is used as a reference for measurements of the binding energies of all photoelectron lines.

State	Binding energy (eV)	Tentative assignment
$4s^{-1}$	9.45 (± 0.05)	
1	15.5 (± 0.1)	$3d^{10}(^1S)4p\,^2P$
$3d^{-1}$	17.29	
3	23.45 (± 0.05)	$3d^9 4s(^3D)4p\,^2P$ or ^2D
5	25.65 (± 0.5)	$3d^9 4s(^1D)4p\,^2P$ or ^2D
6	30.1 (± 0.1)	$3d^9 4s(^1D)4p\,^2P$ or ^2D
		$3d^9 4s(^{1,3}D)5s\,^2D$
		$3d^9 4s(^{1,3}D)4d\,^2D$
		$3d^9(^{1,3}D)4p\,^2P$ or ^2D
		$3d^9 4s(^1D)5p\,^2P$ or ^2D
7	33.5 (± 0.2)	
8	39.0 (± 0.2)	
9	43.8 (± 0.2)	
10	46.3 (± 0.2)	
11	48.6 (± 0.2)	

cesses. The resonant structures are located far above the double-ionization onsets $3d^{10}\,{}^1S$ and $3d^9 4s\,{}^{3,1}D$ and below the double-ionization onsets of $3d^8 4s^2$. They are also located above the singly ionized states with $3p^6 3d^9 4s 4d$ and $3p^6 3d^9 4p^2$ configurations as suggested by the calculations of Cowan and Wilson [22] (see Table II caption). Therefore we suggest that the core-excited states $3p^5 3d^{10} 4s^2 ns$ (or nd) of Zn decay to singly ionized states $3p^6 3d^8 4s^2 nl$ of Zn^+, converging to the $3p^6 3d^8 4s^2$ double-ionization thresholds.

In a second step, the singly ionized resonant satellites *A*, *B*, and *C* may autoionize into the various double continua issued from $3d^{10}\,{}^1S$, $3d^9 4s\,{}^{1,3}D$, or $3d^9 4p\,{}^{3,1}P$, ${}^{3,1}D$, ${}^{3,1}F$ states and give rise to resonant structures within the low-kinetic-energy range. This is shown in Fig. 5. More details are given in the Appendix. The results of our analysis concerning the second-step decay routes (or Auger decay) are given in Table III and in the energy-level diagram of zinc shown in Fig. 6.

(iii) A possible decay route lies in the direct production of Zn^{2+} ions through a resonant shakeoff process. Its existence and intensity have been discussed in several papers [26–28]. In photoelectron spectra this process should be revealed by an increase of the background signal at both extrema of the kinetic-energy scale, i.e., at the zero energy and at the onset of the double continua. This could be the case in zinc, since the resonant structures *A*, *B*, and *C* may couple with the underlying double continua as it has been shown [17] for satellite 6.

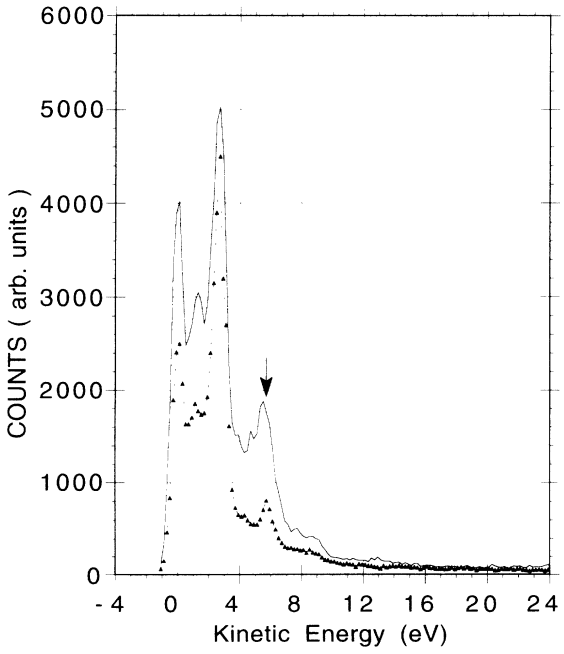

FIG. 5. The low-kinetic-energy scale of the PES shown in Fig. 4 (curves *a* and *d*, respectively). Solid line: PES recorded at 93.90±0.35 eV; open triangle: PES recorded at 90.10±0.35 eV. Both spectra are normalized in position and intensity to the $3d^{-1}$ mainline. The spectra are not corrected for the transmission function of the electron analyzer. In both spectra, the arrow locates the position of the electron energy corresponding to the CKES spectrum displayed in Fig. 2, curve *c*.

Validity of the spectator-electron model

The resonant satellite spectrum emitted upon the decay of the excited state $3p^5({}^2P_{3/2})3d^{10}4s^2 ns$ of Zn should resemble the super-Coster-Kronig electron spectrum of the $3p$ hole ion state Zn^+ $3p^5({}^2P_{3/2})3d^{10}4s^2 \rightarrow 3p^6 3d^8 4s^2({}^1S, {}^1G, {}^3P, {}^1D, {}^3F) + \varepsilon f$, if the excited *ns* electron stayed as a "spectator" in the decay of the $3p$ core hole. Meyer *et al.* [29] have shown that this resemblance to the SCK electron spectrum of the core hole has to be restrained with regard to the multiplet splitting, intensity distribution, and an energy shift due to the presence of the extra excited electron. The SCK electron spectrum of the $3p({}^2P_{3/2,1,2})$ holes recorded at 104.5-eV excitation energy is shown in Fig. 3. It exhibits two peaks separated by ≈ 3 eV at 41.7-eV and 44.7-eV electron energy. The calculated transition ratios [7] to the ${}^1G$, ${}^3F$, and ${}^1D$ dominant multiplet terms are 0.6, 0.28, and 0.07, respectively, and the calculated energies [7] for these same terms relatively to the $3p_{3/2}^{-1}$ (or $3p_{1/2}^{-1}$) level are 40.9 (43.9), 44.3 (47.3), and 42.1 eV (45.1 eV), respectively. In a simple approach, the 5*s* electron staying as a spectator, the

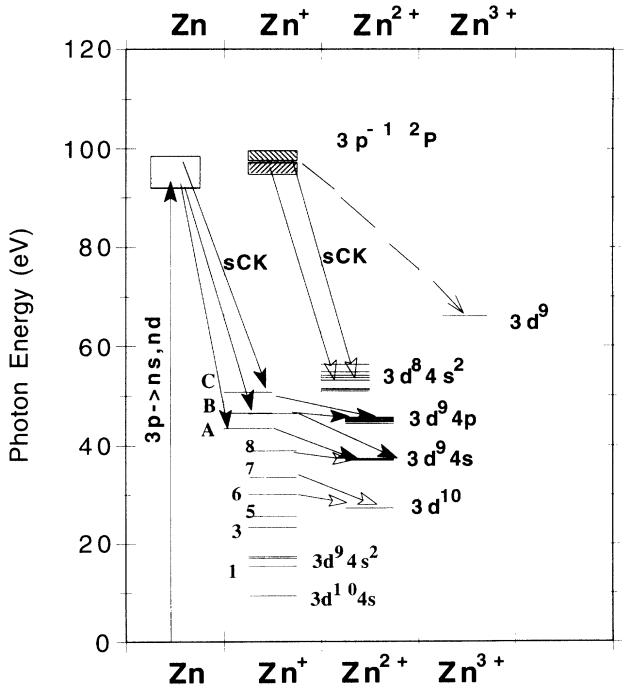

FIG. 6. Energy-level diagram of zinc and its ions with excitation and decay paths of the $3p \rightarrow ns, nd$ resonances. The $3p \rightarrow ns, nd$ transitions lie inside the rectangle when calculated by the $(Z+1)$ model. The hatched rectangles indicate the experimental position of the two $3p^{-1}$ thresholds (see Fig. 2). The levels of the resonant *A*, *B*, and *C* states are given for the 93.9-eV photon energy (see Fig. 4, curves *b* and *c*). The solid arrows show the pathways for the super-Coster-Kronig decay producing doubly charged ions. The open arrows show the off-resonance Auger paths of satellites 6–8 and the super-Coster-Kronig decay of $3p^5 3d^{10} 4s^2({}^2P_{3/2,1/2})$ states. The Zn^{2+} and Zn^{3+} levels are obtained from Moore [21] or Crooker and Dick [23].

TABLE III. Energies of the electron emitted upon the Auger decay of photoelectron satellites 6–11 and the resonant structures *A*, *B*, and *C*. In column 1, the $E_{n,i}$ (eV) are the experimental binding energies. In column 2, the $E_{n,f}$ (eV) are the electron-removal energies for the doubly ionic states with configuration $3d^{10}\varepsilon l,\varepsilon' l'$, $3d^9 4s\varepsilon l,\varepsilon' l'$, and $3d^9 4p\varepsilon l,\varepsilon' l'$ obtained from Moore [21]. We have reported the highest and lowest levels of the numerous multiplet terms corresponding to the $3d^9 4s\varepsilon l,\varepsilon' l'$ and $3d^9 4p\varepsilon l,\varepsilon' l'$ configurations. Within these conditions we neglect any selection rule for the Auger decay and we may expect Auger-electron lines in energy intervals displayed in column 3. Comparing the data displayed in column 3 and the PES reported in Fig. 5, we have selected the most probable Auger lines on the right-hand side of column 3.

	Electron lines		Zn^{2+} states		Electron energy	
States	$E_{n,i}$ (eV)	Width (eV)	$E_{n,f}$ (eV)	Configuration	(eV)	
6	30.1 (±0.1)	1 (±0.1)	27.35	$3d^{10}$		≈2.75
7	33.5 (±0.2)		27.35	$3d^{10}$		≈5.9
8	39.0 (±0.2)		27.35	$3d^{10}$	≈11.65	
			37–37.7	$3d^9 4s$		≈1.3–2
9	43.8 (±0.2)		27.35	$3d^{10}$	≈16.5	
			37–37.7	$3d^9 4s$		≈6.1–6.8
A	43.3 (±0.2)		27.35	$3d^{10}$	≈16	
			37–37.7	$3d^9 4s$		≈6–6.4
B	46.60 (±0.1)	1.6 (±0.1)	27.35	$3d^{10}$	≈19.15	
			37–37.7	$3d^9 4s$		≈8.9–9.6
			44.4–45.7	$3d^9 4p$		≈0.9–2.2
C	50.7 (±0.2)	1.6 (±0.2)	27.35	$3d^{10}$	≈23.35	
			37–37.7	$3d^9 4s$	≈13.0–13.7	
			44.4–45.7	$3d^9 4p$		≈5–6.3

$3p^5(^2P_{3/2})3d^{10}4s^2 5s\ ^1P$ state excited at 92-eV photon energy could decay into the singly ionized states

$$3p^6 3d^8 4s^2(^1S,^1G,^3P,^1D,^3F)5s\,(^2S,^2G,^2P,^4P,^2D,^2F,^4F)\ ,$$

and we would expect the ^2G and $^2F,^4F$ *LS*-coupling multiplet terms to be the components of the resonant satellites *B* and *A* (curve *b*) in Fig. 4 (the interval energy between the two lines *A* and *B* is ≈3 eV). Nevertheless, at 94.2-eV photon energy the expected $3p \rightarrow 6s$ transition also produces a strong *B* line. Also at 93.1 eV, the *C* resonant structure characteristic of the $3p \rightarrow 6s$ transition is already appearing. Thereby we conclude that the resonant satellites spectra shown in Fig. 4 (curves *a*–*e*) are apparently more complex than one could expect from a simple spectator-electron model.

An important remark concerns the breakdown of the spectator-electron approximation when considering the super-Coster-Kronig decay of the excited states $3p^5(^2P_{3/2,1/2})3d^{10}4s^2 ns\ ^{3,1}P_1$ into the various ionic states $3p^6 3d^8 4s^2 ns$. In fact, because of the spreading of the ionic states ($3d^8 ns$) over a large energy range and the mixing of $^1P_1$ and $^3P_1$ components in the excited states, a different description for the *ns* electron has to be used, according to the excited and ionic states considered.

We also suggest that the almost similarity of the spectra in Fig. 4 (curves *c*–*e*) could be due to (a) the participation of the excited electron to the super-Coster-Kronig decay of the 3*p* core hole:

$$3p^5(^2P_{3/2,1/2})3d^{10}4s^2 ns\ ^{3,1}P_1 \rightarrow 3p^6 3d^8 4s^2 n'l\varepsilon f$$

with $n' \geq n$ (such an effect, but weaker, has already been observed by Meyer *et al.* [30] in case of Ni) or (b) the overlapping of the $3p \rightarrow ns$ excited states in the series.

CONCLUSION

In conclusion, we brought evidence of the extensive role played by the $3p^{-1}ns^1 \rightarrow 3d^{-2}n'l'\varepsilon f$ $(n \geq n)$ super-Coster-Kronig processes upon the decay of excited states in zinc in the 3*p* thresholds region. As a consequence we have pointed out the existence of an important indirect double-ionization process below the 3*p* ionization onsets in addition to the normally expected shakeoff effect and a large broadening of these 3*p* excited states which form series of overlapping states, rendering inappropriate the characterization as "Rydberg" series of excited states. Moreover, we have put in light different broadenings when we compare the linewidths in the case of the 3*p* hole decay after excitation or ionization in both copper and zinc.

ACKNOWLEDGMENTS

The authors would like to warmly thank L. Hellner and G. Dujardin for experimental support. They also would like to thank M. Ohno for helpful discussions. The authors acknowledge J. M. Bizau and D. Cubaynes in the managing of the monochromator and beam line. They are grateful to the Laboratoire pour l' Utilisation du Rayonnement Electromagnétique and the Laboratoire de l'Accélérateur Linéaire for financial and technical support. The foundation Interuniverstario Nationale per la Fisisca della Materia is also acknowledged for financial support.

APPENDIX

The first threshold for the double continuum with the $3d^{10}\,{}^1S$ configuration lies at a 27.35-eV energy just between satellites 5 and 6 (see Fig. 3 and the energy-level diagram of Fig. 6). Therefore satellites 6–11 autoionize into double continua to produce doubly charged ions whereas the $4s^{-1}$, $3d^{-1}$, and satellite 5 produce Zn^+ ions. Details in the low-kinetic-energy scale of the PES spectra recorded at 90.10±0.35 and 93.90±0.35 eV are reported in Fig. 5. The huge peak at 2.7 eV corresponds to the electrons emitted upon the autoionization [17] of satellite 6 into the double continuum with $3d^{10}\,{}^1S$ configuration, and the small peak observed at 5.8 eV could correspond to the autoionization of satellites 7 and 9. The complete decay process of the $3p$ core-excited states produces two electrons as shown:

$$
\begin{aligned}
&3p^6 3d^{10} 4s^2 + h\nu \\
&\quad \rightarrow 3p^5({}^2P_{3/2} \text{ or } {}^2P_{1/2}) 3d^{10} 4s^2 ns(\text{or } nd) \\
&\quad \rightarrow 3p^6 3d^8 4s^2 nl + e_1^-(\text{SCK}) \\
&\quad \rightarrow 3p^6 3d^9 4s(\text{or } 4p) + e_1^-(\text{SCK}) + e_2^-(\text{Auger}) \,. \qquad \text{(A1)}
\end{aligned}
$$

The electrons e_2^-(Auger) emitted upon the second-step Auger decay should be detected in the low-kinetic-energy range of the PES, and these Auger lines may be superimposed on the Auger lines due to the autoionization of satellites 6–11.

We have reported in Table III the possible Auger-electron energies. The arrows in the level diagram (Fig. 6) indicate the conclusions we draw from the comparison of Table III and the PES displayed in Fig. 5. On resonance, at 93.9 eV, a stronger peak appears at 5.5 eV. This resonant Auger line may be due either to the autoionization of the satellite C into the double continua with the $3d^9 4p\varepsilon l, \varepsilon' l'$ configuration, or to the autoionization of the satellite A into the double continua with the $3d^9 4s\varepsilon l, \varepsilon' l'$ configuration. According to this analysis, we may explain the first large structure shown in the 91–97-eV energy region of the constant-kinetic-energy spectrum, curve C in Fig. 2. The CKES spectrum was recorded with a monochromator band pass varying between 0.3 and 0.5 eV as the photon energy was scanned in the 82–112-eV range, and the energy resolution of the analyzer was set at 0.7 eV. Therefore the CKES displays the number of electrons with energy roughly in the 5.2–6.1-eV range. The enhancement of the CKES observed in the 91–97-eV photon energy region reveals the fact that we should observe resonant satellites A and C in PES, as the excitation energy of the PES is scanned between 91 and 97 eV; this is in agreement with the spectra reported in Fig. 4.

When comparing the low-kinetic-energy spectra of Fig. 5 obtained at 93.9 eV to high-energy spectra (curve d) in Fig. 4, we explain the enhancement of the on-resonance PES at kinetic energies around 1.4 and 9 eV, respectively. In fact, the most intense resonant line (satellite B) may autoionize into either the $3d^9 4p\varepsilon l, \varepsilon' l'$ or the $3d^9 4s\varepsilon l, \varepsilon' l'$ double continua.

[1] B. Sonntag and P. Zimmermann, Rep. Prog. Phys. **55**, 911 (1992).

[2] L. C. Davis and L. A. Feldkamp, Phys. Rev. A **24**, 1862 (1981).

[3] F. Combet Farnoux, Z. Phys. D **2**, 337 (1986).

[4] D. Chandesris, C. Guillot, G. Chauvin, J. Lecante, and Y. Petroff, Phys. Rev. Lett. **47**, 1273 (1981).

[5] R. Bruhn, E. Schmidt, H. Schröder, and B. Sonntag, J. Phys. B **15**, L441 (1982).

[6] A. Dadouch, S. Stranges, M. Y. Adam, L. Hellner, G. Dujardin, and F. Combet Farnoux, Phys. Rev. A **43**, 1648 (1991).

[7] M. Ohno and G. Wendin, J. Phys. B **12**, 1305 (1979).

[8] T. Hayaishi, Y. Morioka, T. Akahori, M. Watanabe, A. Yagishita, and M. Nakamura, Z. Phys. D **4**, 25 (1986).

[9] W. Mehlhorn, B. Breuckmann, and D. Hausamann, Phys. Scr. **16**, 177 (1977).

[10] M. H. Chen, B. Crasemann, M. Aoyagi, and H. Mark, Phys. Rev. A **18**, 802 (1978).

[11] A. W. Fliflet and H. P. Kelly, Phys. Rev. A **13**, 312 (1976).

[12] M. W. D. Mansfield and J. P. Connerade, Proc. R. Soc. London Ser. A **359**, 389 (1978).

[13] H. Harrison, R. I. Schoen, R. B. Cairns, and K. E. Schubert, J. Chem. Phys. **50**, 3930 (1969).

[14] R. B. Cairns, H. Harrison, and R. I. Schoen, J. Chem. Phys. **51**, 5440 (1969).

[15] D. M. P. Holland, K. Codling, and J. B. West, J. Phys. B **15**, 1473 (1982).

[16] S. Stranges, S. Svensson, and M. Y. Adam (unpublished).

[17] S. Svensson, S. Stranges, and M. Y. Adam, Phys. Rev. A **48**, 3051 (1993).

[18] W. A. Johnson, V. Radojevic, P. Deshmukh, Phys. Rev. A **25**, 337 (1982).

[19] P. Morin, M. Y. Adam, J. Delwiche, M. J. Hubin-Franskin, I. Nenner, and P. Lablanquie, Nucl. Instrum. Methods **208**, 761 (1983).

[20] M. Y. Adam, L. Hellner, G. Dujardin, A. Svensson, P. Martin, and F. Combet Farnoux, J. Phys. B **22**, 2141 (1982).

[21] C. E. Moore, *Atomic Energy Levels,* Natl. Bur. Stand. (U.S.) Circ. No. 567 (U.S. GPO, Washington, D.C., 1958).

[22] R. D. Cowan and M. Wilson, J. Phys. B **21**, 275 (1988).

[23] A. M. Crooker and K. A. Dick, Can. J. Phys. **46**, 1241 (1968); K. A. Dick, *ibid.* **46**, 1291 (1968).

[24] E. Jensen, R. A. Bartynski, S. L. Hulbert, E. D. Johnson, and R. Garrett, Phys. Rev. Lett. **62**, 1273 (1981).

[25] R. Bruhn, E. Schmidt, H. Schröder, and B. Sonntag, J. Phys. B **15**, 71 (1989).

[26] U. Becker, D. Szostak, M. Kupsch, H. G. Kerkhoff, B. Langer, and R. Wehlitz, J. Phys. B **22**, 749 (1989).

[27] T. Hayaishi, Y. Morioka, Y. Kageyama, M. Watanabe, I. H. Suzuki, A. Mikuni, G. Isoyama, S. Asaoka, and M. Nakamura, J. Phys. B **17**, 3511 (1984).

[28] P. A. Heimann, D. W. Lindle, T. A. Ferrett, S. H. Liu, L.

J. Medhurst, M. N. Piancastelli, D. A. Shirley, U. Becker, H. G. Kerkhoff, B. Langer, D. Szostak, and R. Wehlitz, J. Phys. B **20**, 5005 (1987).

[29] M. Meyer, E. Von Raven, M. Richter, B. Sonntag, and J. E. Hansen, J. Electron Spectrosc. Relat. Phenom. **51**, 407 (1990).

[30] M. Meyer, Th. Prescher, E. von Raven, M. Richter, E. Schmidt, B. Sonntag, and H. E. Wetzel, Z. Phys. D **2**, 347 (1986).